

Spatially dependent flood probabilities to support the design of civil infrastructure systems

Phuong Dong Le^{1,2}, Michael Leonard¹, Seth Westra¹

¹*School of Civil, Environmental and Mining Engineering, University of Adelaide, Adelaide, South Australia, Australia*

²*Thuyloi University, 175 Tay Son, Dong Da, Hanoi, Vietnam*

Email: lephuongdong_tb@tlu.edu.vn

Keywords: areal reduction factor, asymptotic independence, conditional probability, duration dependence, extreme rainfall, flood probability, inverted max-stable process, joint probability, spatially dependent Intensity-Duration-Frequency

Abstract

Conventional flood risk methods typically focus on estimation at a single location, which can be inadequate for civil infrastructure systems such as road or railway infrastructure. This is because rainfall extremes are spatially dependent, so that to understand overall system risk it is necessary to assess the interconnected elements of the system jointly. For example, when designing evacuation routes it is necessary to understand the risk of one part of the system failing given that another region is flooded or exceeds the level at which evacuation becomes necessary. Similarly, failure of any single part of a road section (e.g., a flooded river crossing) may lead to the wider system's failure (i.e. the entire road becomes inoperable). This study demonstrates a spatially dependent Intensity-Duration-Frequency framework that can be used to estimate flood risk across multiple catchments, accounting for dependence both in space and across different critical storm durations. The framework is demonstrated via a case study of a highway upgrade, comprising five river crossings. The results show substantial differences in conditional and unconditional design flow estimates, highlighting the importance of taking an integrated approach. There is also a reduction in the estimated failure probability of the overall system compared with the case where each river crossing is treated independently. The results demonstrate the potential uses of spatially dependent Intensity-Duration-Frequency methods and suggest the need for more conservative design estimates to take into account conditional risks.

29 **1. Introduction**

30 Methods for quantifying the flood risk of civil infrastructure systems such as road and rail networks
31 require considerably more information compared to traditional methods that focus on flood risk at a
32 point. For example, the design of evacuation routes requires the quantification of the risk that one part
33 of the system will fail at the same time that another region is flooded or exceeds the level at which
34 evacuation becomes necessary. Similarly, a railway route may become impassable if any of a number
35 of bridges are submerged, such that the ‘failure probability’ of that route becomes some aggregation of
36 the failure probabilities of each individual section. Successful estimation of flood risk in these systems
37 therefore requires recognition both of the networked nature of the civil infrastructure system across a
38 spatial domain, as well as the spatial and temporal structure of flood-producing mechanisms (e.g. storms
39 and extreme rainfall) that can lead to system failure (e.g., [Leonard et al. \(2014\)](#), [Seneviratne et al.
40 \(2012\)](#), [Zscheischler et al. \(2018\)](#)).

41 One way to estimate such flood probabilities is to directly use information contained in historical
42 streamflow data. For example, annual maximum streamflow at two locations might be assumed to
43 follow a bivariate generalized extreme value distribution ([Favre et al., 2004](#); [Wang, 2001](#); [Wang et al.,
44 2009](#)), which can then be used to estimate both conditional probabilities (e.g. the probability that one
45 river is flooded given that the other river level exceeds a specified threshold) and joint probabilities
46 (e.g. the probability that one or both rivers are flooded). Several frameworks have been demonstrated
47 based directly on streamflow observations, including functional regression ([Requena et al., 2018](#)),
48 multisite copulas ([Renard and Lang, 2007](#)), and spatial copulas ([Durocher et al., 2016](#)). However, in
49 many instances continuous streamflow data are unavailable or insufficient at the locations of interest,
50 or the catchment conditions have changed such that historical streamflow records as unrepresentative
51 of likely future risk. For these situations, rainfall-based methods are often more appropriate.

52 There are two primary classes of rainfall-based methods to estimate flood probability. The first uses
53 continuous rainfall data (either historical or generated) to compute continuous streamflow data using a
54 rainfall-runoff model ([Boughton and Droop, 2003](#); [Cameron et al., 1999](#); [He et al., 2011](#); [Hegnauer et
55 al., 2014](#); [Pathiraja et al., 2012](#)), with flood risk then estimated based on the simulated streamflow time

56 series. This method is computationally intensive and given the challenge of reproducing a wide variety
57 of statistics across many scales, can have difficulties in modelling the dependence of extremes. Most
58 spatial rainfall models operate at the daily timescale ([Bárdossy and Pegram, 2009](#); [Baxevani and](#)
59 [Lennartsson, 2015](#); [Bennett et al., 2016b](#); [Hegnauer et al., 2014](#); [Kleiber et al., 2012](#); [Rasmussen, 2013](#)),
60 whereas many catchments respond at sub-daily timescales. This is likely because the capacity of space-
61 time rainfall models to simulate the statistics of sub-daily rainfall remains a challenging research
62 problem ([Leonard et al., 2008](#)), although one approach is to exploit the relative abundance of data at
63 the daily scale, then apply a downscaling model to reach sub-daily scales ([Gupta and Tarboton, 2016](#)).
64 Continuous simulation is receiving ongoing attention and increasing application, yet there remain
65 limitations when applying these models in many practical contexts.

66 The second rainfall-based method proceeds by applying probability calculations on rainfall, to construct
67 ‘Intensity-Duration-Frequency’ (IDF) curves, which are then translated to a runoff event of equivalent
68 probability either via empirical models such as the rational method to estimate peak flow rate
69 ([Kuichling, 1889](#); [Mulvaney, 1851](#)), or via event-based rainfall-runoff models that are able to simulate
70 the full flood hydrograph ([Boyd et al., 1996](#); [Chow et al., 1988](#); [Laurenson and Mein, 1997](#)). Regional
71 frequency analysis is one type of method to estimate IDF values, where the precision of at-site estimates
72 is improved by pooling data from sites in the surrounding region ([Hosking and Wallis, 1997](#)). These
73 methods can be combined with spatial interpolation methods to estimate parameters for any ungauged
74 location of interest ([Carreau et al., 2013](#)). To determine an effective mean depth of rainfall over a
75 catchment with the same exceedance probability as at a gauge location, the pointwise estimate of
76 extreme rainfall is multiplied by an areal reduction factor (ARF) ([Ball et al., 2016](#)). However, such
77 methods do not account for information on the spatial dependence of extreme rainfall—whether for a
78 single storm duration, or for the more complex case of different durations across a region ([Bernard,](#)
79 [1932](#); [Koutsoyiannis et al., 1998](#)). The underlying independence assumption prevents these approaches
80 from being applied to estimate conditional or joint flood risk at multiple points in a catchment or across
81 several catchments, as would be required for a civil infrastructure system.

82 Although multivariate approaches can be tailored to estimate conditional and joint probabilities of
83 extreme rainfall for specific situations (e.g., [Kao and Govindaraju \(2008\)](#), [Wang et al. \(2010\)](#), [Zhang
84 and Singh \(2007\)](#)), the development of a unified methodology that integrates with existing IDF-based
85 flood estimation approaches remains elusive. This is particularly challenging given that it is not only
86 necessary to account for dependence of rainfall across space, but also to account for dependence across
87 storm burst durations, as different parts of the system may be vulnerable to different critical duration
88 storm events. To this end, max-stable process theory has been demonstrated to represent storm-level
89 dependence ([de Haan, 1984](#); [Schlather, 2002](#)) and used to calculate conditional probabilities for a spatial
90 domain ([Padoan et al., 2010](#)). Max-stable process has also been used to represent the co-occurrence of
91 extreme daily rainfall in the French Mediterranean region ([Blanchet and Creutin, 2017](#)). Copulas
92 including the extremal-t copula ([Demarta and McNeil, 2005](#)), and the Husler-Reiss copula ([Hüsler and
93 Reiss, 1989](#)) have also been used to model rainfall dependence.

94 This study applies a max-stable approach with an emphasis on practical flood estimation problems. To
95 this end, any proposed approach needs to account for:

- 96 1. The spatial dependence of rainfall ‘events’ both for single durations, and also across multiple
97 different durations. This was addressed by [Le et al. \(2018b\)](#), who linked a max-stable model
98 with the duration-dependent model of [Koutsoyiannis et al. \(1998\)](#), to create a model that could
99 be used to reflect dependencies between nearby catchments of different sizes.
- 100 2. The asymptotic properties of spatial dependence as the events become increasingly extreme,
101 given the focus of many flood risk estimation methods on rare flood events. Recent evidence is
102 emerging that rainfall has an asymptotically independent characteristic ([Le et al., 2018a](#);
103 [Thibaud et al., 2013](#)), which means that the level of the rainfall’s dependence reduces with an
104 increasing return period ([Wadsworth and Tawn, 2012](#)). The requirement of asymptotic
105 independence indicates that inverted max-stable models are preferable over max-stable models.

106 This study adapts the methods developed by [Le et al. \(2018b\)](#) to inverted max-stable models to derive
107 spatially-dependent IDF estimates and ARFs as the basis for transforming rainfall into flood flows. The
108 approach is demonstrated on a highway system spanning 20 km with five separate river crossings.

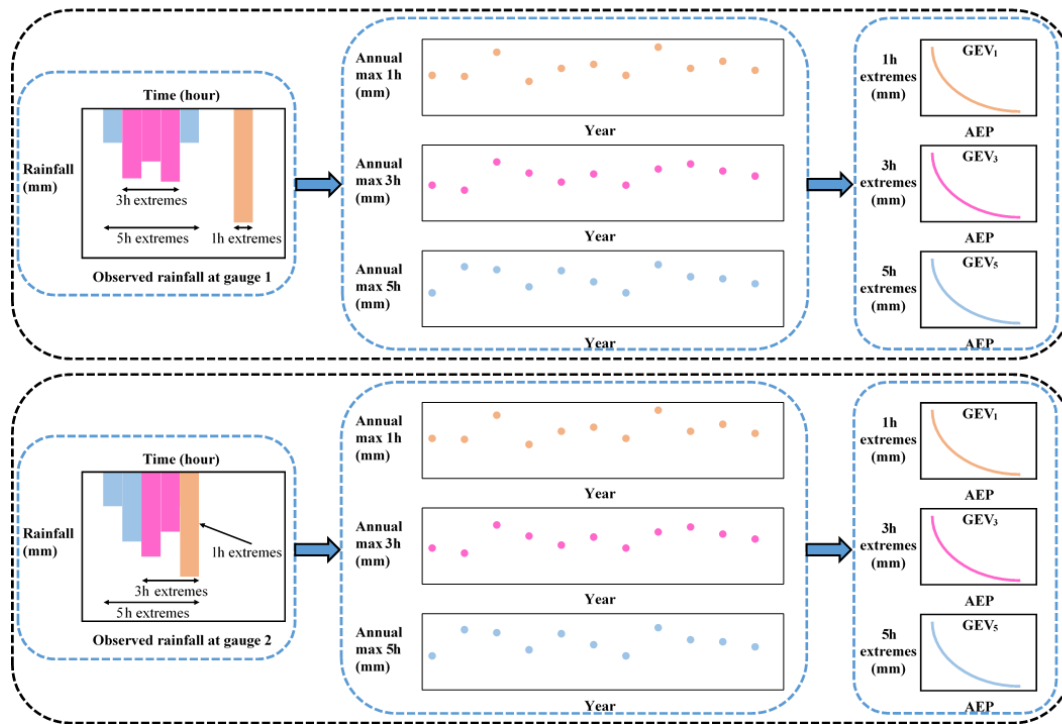
109 The case study is designed to address two related questions: (i) “What flood flow needs to be used to
110 design a bridge that will fail on average only once on average every M times given that a neighbouring
111 catchment is flooded?”; and (ii) “What is the probability that the overall system fails given that each
112 bridge is designed to a specific exceedance probability event (e.g., the 1% annual exceedance
113 probability event)?” The method for resolving these questions represents a new approach to estimate
114 flood risk for engineering design, by focusing attention on the risk of the entire system, rather than the
115 risk of individual system elements in isolation.

116 In the remainder of the paper, Section 2 emphasises the need for spatially dependent IDF estimates in
117 flood risk design, followed by Section 3 which outlines the case study and data used. Section 4 explains
118 the implementation of the framework, including a method for analysing the spatial dependence of
119 extreme rainfall across different durations. Results on the behaviour of floods due to the spatial and
120 duration dependence of rainfall extremes, are provided in Section 5. Conclusions and discussion follow
121 in Section 6.

122 **2. The need for spatially dependent IDF estimates in flood risk estimation**

123 The main limitation of conventional methods of flood risk estimation is that they isolate bursts of
124 rainfall and break the dependence structure of extreme rainfall. Figure 1 demonstrates a traditional
125 process of estimating at-site extreme rainfall for two locations (gauge 1, gauge 2) and three durations
126 (1, 3, and 5 hr) ([Stedinger et al., 1993](#)). The process first involves extracting the extreme burst of rainfall
127 for each site, duration and year from the continuous rainfall data, and then fitting a probability
128 distribution (such as the Generalised Extreme Value (GEV) distribution) to the extracted data. Figure 1
129 demonstrates that, through the process of converting the continuous rainfall data to a series of discrete
130 rainfall ‘bursts’, this process breaks the dependence both with respect to duration and space. Firstly, the
131 duration dependence is broken by extracting each duration separately, whereas for the hypothetical
132 storm in Fig. 1 it is clear that the annual maxima from some of the extreme bursts come from the same
133 storm. Secondly, the spatial dependence is broken because each site is analysed independently. Again,
134 for the hypothetical storm of Fig. 1 it can be seen that the 5 hr storm has occurred at the same time
135 across the two catchments, and this information is lost in the subsequent probability distribution curves.

136 Lastly, there is cross-dependence in space and duration. For example, the 1 hr extreme from gauge 2
 137 occurs at the same time as the 5 hr extreme from gauge 1. This may be relevant if there are two
 138 catchments with times of concentration matching 1 hr and 5 hr respectively, which can arise where
 139 catchments are neighbouring or nested.

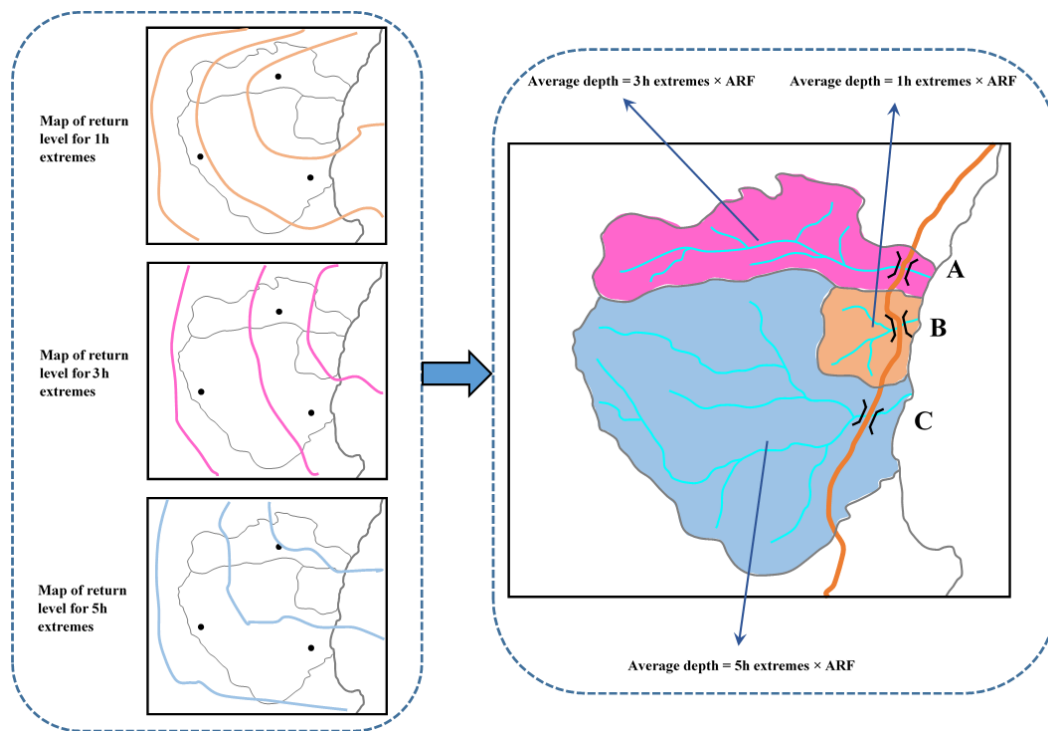


140
 141 **Figure 1.** Illustration of process to estimate rainfall extremes for each individual location in conventional flood risk
 142 approach, the upper panel is for gauge 1 and the lower panel is for gauge 2.

143 Having obtained the IDF estimates for individual locations in Fig. 1, the next step is commonly to
 144 convert this to spatial IDF maps by interpolating results between gauged locations. Figure 2 shows
 145 hypothetical IDF maps from individual sites, with a separate spatial contour map usually provided for
 146 each storm burst duration. In a conventional application the respective maps are used to estimate the
 147 magnitude of extreme rainfall over catchments for a specified time of concentration. The IDF estimates
 148 are combined with an areal reduction factor (ARF) to determine the volume of rainfall over a region
 149 (since rainfall is not simultaneously extreme at all locations over the region). However, because the
 150 spatial dependence was broken in the IDF analysis, the ARFs come from a separate analysis and are an
 151 attempt to correct for the broken spatial relationship within a catchment ([Bennett et al., 2016a](#)). Lastly,
 152 the rainfall volume over the catchment is combined with a temporal pattern (i.e. the distribution of the

153 rainfall hyetograph within a single ‘storm burst’) and input to a runoff model to simulate flood-flow at
154 a catchment’s outlet. Where catchment flows can be considered independently this process has been
155 acceptable for conventional design, but because this process does not account for dependence across
156 durations and across a region, it is not possible to address problems that span multiple catchments, as
157 with civil infrastructure systems.

158



159

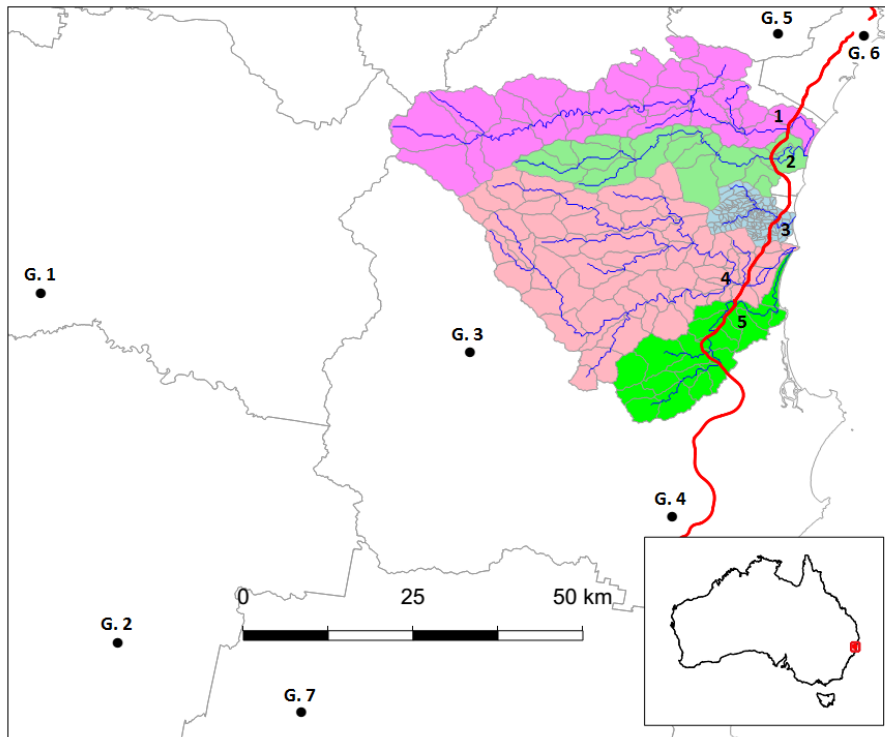
160 **Figure 2.** Illustration of map of return level and how to use it in estimating flood flow in conventional flood risk estimates
161 approach.

162 The process in Fig. 1 breaks out the dependence of the observed rainfall, which makes the conventional
163 approach unable to analyse the dependence of flooding at two or more separate locations. Instead, this
164 paper advocates for spatially dependent IDF estimates that are developed by retaining the dependence
165 of observed rainfall in the estimation of extremal rainfall. By applying spatially dependent IDF
166 estimates to a rainfall-runoff model, it becomes possible to represent the dependence of flooding
167 between separate locations.

168 3. Case study and data

169 The region chosen for the case study is in the mid north coast region of New South Wales, Australia.
170 This region has been the focus of a highway upgrade project and has an annual average daily traffic
171 volume on the order of 15,000 vehicles along the existing highway. The upgrade traverses a series of
172 coastal foothills and floodplains for a total length of approximately 20 km. The project's major river
173 crossings consist of extensive floodplains with some marsh areas.

174 The case study has five main catchments that are numbered in sequence in Fig. 3: (1) Bellinger, (2)
175 Kalang River, (3) Deep Creek, (4) Nambucca and (5) Warrell Creek. The area and time of concentration
176 of these catchments is summarised in Table 1, with the latter estimated using the ratio of the flow path
177 length and average flow velocity ([SKM, 2011](#)). The Deep Creek catchment has a time of concentration
178 of 8 hr, while the other four catchments have much longer times of concentration, ranging from 27 to
179 38 hr. The differing durations indicate that it is necessary to consider spatial dependence across this
180 range of durations to estimate joint and conditional flood risk. The spatial dependence across rainfall
181 durations is expected to be lower than across a single duration, since short- and long-rain events are
182 often driven by different meteorological mechanisms ([Zheng et al., 2015](#)). However some spatial
183 dependence is still likely to be present, given that extremal rainfall in the region is strongly associated
184 with 'east coast low' systems off the eastern coastline, whereby extreme hourly rainfall bursts are often
185 embedded in heavy multi-day rainfall events.



186

187 **Figure 3.** Map of the case study in New South Wales, Australia. The black dots indicate the rainfall gauges (G. 1 to G. 7),
 188 the red line indicates the Pacific Highway upgrade project, and the blue lines indicate the main river network. The numbers
 189 from one to five indicate the locations of the main river crossings.

190

Table 1. Summary of case study catchments properties.

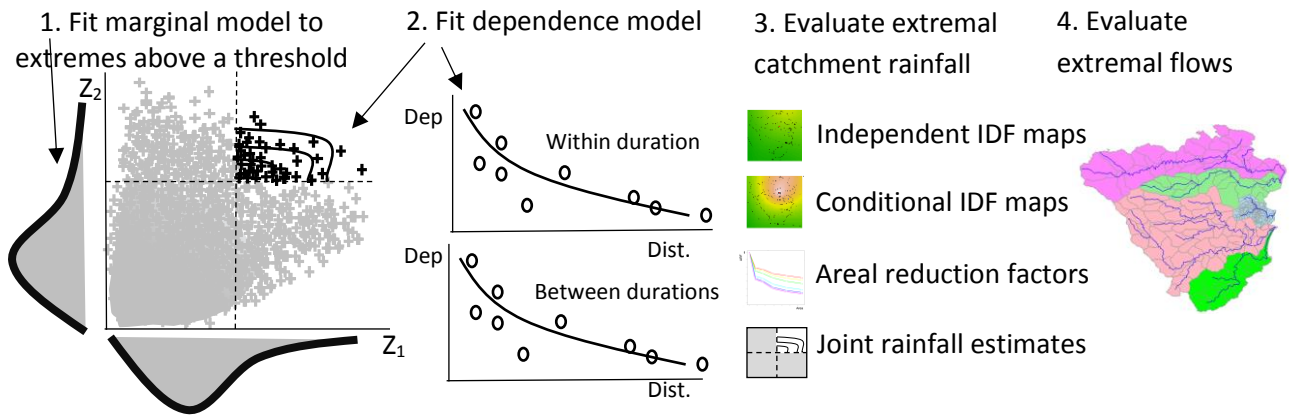
No.	Catchment	Area (km ²)	Time of concentration (hour)
1	Bellinger	772	37
2	Kalang River	341	33
3	Deep Creek	92	8
4	Nambucca (upper)	1020	38
5	Warrell Creek	294	27

191 The black circles in Fig. 3 represent the sub-daily rain stations used for this study. There were seven
 192 sub-daily stations selected, with 35 years of record in common for the whole region. The data was
 193 available at a 5 minute interval and aggregated to longer durations. For convenience in comparing the
 194 times of concentration between the catchments, this study assumes a time of concentration of 9 hr for
 195 the Deep Creek catchment, while identical times of concentration of 36 hr are assumed for the other
 196 four catchments.

197

198 **4. Methodology**

199 This section describes the method used to estimate the conditional and joint probabilities of streamflow
 200 for civil infrastructure systems based on rainfall extremes, with the sequence of steps illustrated in Fig.
 201 4. The overall aim is to estimate rainfall exceedance probabilities and corresponding flow estimates that
 202 account for dependence across multiple catchments. The generalized Pareto distribution (GPD) is used
 203 as the marginal distribution to fit to observed rainfall above some large threshold for all durations at
 204 each location (Section 4.1). An extremal dependence model is required to evaluate conditional and joint
 205 probabilities. Here, an inverted max-stable process is used with dependence not only in space but also
 206 in duration (Section 4.2). The fitted model is evaluated in a range of contexts, including the construction
 207 of joint and conditional return level maps. The derivation of areal reduction factors and joint rainfall
 208 estimates are made with the assistance of simulations based on the fitted model (Section 4.3). An event-
 209 based rainfall-runoff model is employed in Section 4.4 to transform extremal design rainfalls to
 210 corresponding flows.



211

212 **Figure 4.** The flow chart for the overall methodology.

213 **4.1. Marginal model for rainfall**

214 This study defines extremes as those greater than some threshold u . For large u , the distribution of Y
 215 conditional on $Y > u$ may be approximated by the generalized Pareto distribution (GPD) ([Pickands,](#)
 216 [1975](#); [Davison and Smith, 1990](#); [Thibaud et al., 2013](#)):

217
$$G(y) = 1 - \left\{ 1 + \frac{\xi(y - u)}{\sigma_u} \right\}^{-1/\xi}, \quad y > u, \quad (1)$$

218 defined on $\{y: 1 + \xi(y - u)/\sigma_u > 0\}$ where $\sigma_u > 0$ and $-\infty < \xi < +\infty$ are scale and shape
219 parameters, respectively. The probability that a level y is exceeded is $\Phi_u\{1 - G(y)\}$, where $\Phi_u =$
220 $\Pr(Y > u)$.

221 The selection of the appropriate threshold u involves a trade-off between bias and variance. A threshold
222 that is too low leads to bias because the GPD approximation is poor. A threshold too high leads to high
223 variance because of a small number of excesses. Two diagnostic tests are used to determine the
224 appropriate threshold u : the mean residual life plot and the parameter estimate plot ([Coles, 2001](#);
225 [Davison and Smith, 1990](#)). These methods use the stability property of a GPD, so that if a GPD is valid
226 for all excesses above u , then excesses of a threshold greater than u should also follow a GPD ([Coles](#)
227 [\(2001\)](#)). To construct IDF maps across the region, the parameters of the GPD are interpolated across the
228 region using a thin plate spline with covariates of longitude and latitude. Though more detailed
229 modelling of covariates could be used to improve estimates ([Le et al. \(2018b\)](#)), the interpolation used
230 here is sufficient for demonstrating the overall method.

231 **4.2. Dependence model for spatial rainfall**

232 Consider rainfall as a stationary stochastic process Z_i associated with a location x_i and a specific
233 duration (the notation is simplified from $Z(x_i)$ to Z_i). An important property of dependence in the
234 extremes is whether or not two variables are likely/unlikely to co-occur as the extremes become rarer,
235 as this can significantly influence the estimate of frequency for flood events of large magnitude. This
236 is referred to as asymptotic dependence/independence, respectively. For the case of asymptotic
237 independence, the dependence structure becomes weaker as the extremal threshold increases, which is
238 defined as $\lim_{z \rightarrow \infty} P\{Z_1 > z | Z_2 > z\} = 0$ for all $x_1 \neq x_2$. The spatial extent of a rainfall event with
239 asymptotically independent extremes will diminish as its rarity increases. This study uses an
240 asymptotically independent model, of which multiple types are valid including the Gaussian copula
241 ([Davison et al., 2012](#)) and inverted max-stable processes ([Wadsworth and Tawn, 2012](#)). The inverted
242 max-stable model was ultimately selected in this study to provide consistency earlier research ([Le et](#)
243 [al., 2018a](#)), in which it was demonstrated to preserve the spatial properties of extreme rainfall in an
244 Australian context, including the property of asymptotic independence. [Thibaud et al. \(2013\)](#) also

245 compared the inverted max-stable model with a Gaussian copula in a case study in Switzerland, and
 246 identified that the inverted max-stable model was appropriate.

247 The dependence structure of the inverted max-stable process is represented by the pairwise residual tail
 248 dependence coefficient ([Ledford and Tawn, 1996](#)). For a generic continuous process Z_i for a given
 249 duration and associated with a specific location x_i , the empirical pairwise residual tail dependence
 250 coefficient η for each pair of locations (x_1, x_2) is

$$251 \quad \eta(x_1, x_2) = \lim_{z \rightarrow \infty} \frac{\log P\{Z_2 > z\}}{\log P\{Z_1 > z, Z_2 > z\}}. \quad (2)$$

252 The value of $\eta \in (0,1]$ indicates the level of extremal dependence between Z_1 and Z_2 ([Coles et al.,](#)
 253 [1999](#)), with lower values indicating lower dependence. An example of how to calculate the residual tail
 254 dependence coefficient is provided in Appendix A for a sample dataset. To estimate the dependence
 255 structure of an inverted max-stable model, the theoretical residual tail dependence coefficient function
 256 is fitted to its empirical counterpart. Here the residual tail dependence coefficient function is assumed
 257 to only depend on the Euclidean distance between two locations $h = \|x_1 - x_2\|$. The theoretical
 258 residual tail dependence coefficient function for the inverted Brown-Resnick model is given as:

$$259 \quad \eta(h) = \frac{1}{2\Phi\left\{\sqrt{\frac{\gamma(h)}{2}}\right\}}, \quad (3)$$

260 where Φ is the standard normal cumulative distribution function, h is the distance between two
 261 locations, and $\gamma(h)$ belongs to the class of variograms $\gamma(h) = \|h\|^\beta/q$ for $q > 0$ and $\beta \in (0,2)$. The
 262 model is fitted to the empirical residual tail dependence coefficient by modifying parameters q and β
 263 until the sum of squared errors is minimized.

264 When the extreme rainfall at location x_1 and x_2 are of different durations, the dependence is less than
 265 when the extremes are of the same duration. For example, at a single location ($h = 0$), when the duration
 266 is the same, the rainfall values are identical and have perfect dependence, but when the duration of
 267 extremes are different the values are not identical and the dependence is less. An adjustment needs to

268 be made to the theoretical pairwise residual tail dependence coefficient function when extreme rainfalls
269 have different durations.

270 Following [Le et al. \(2018b\)](#), an adjusted approach is used by adding a nugget to the variogram as:

$$271 \quad \gamma_{ad}(h) = h^\beta / q + c(D - d)/d, \quad (4)$$

272 where h , β , and q are the same as those in Eq. (3); d is the duration (in hours); $0 < d \leq D$, where D is
273 the maximum duration of interest (e.g. $D = 36$ hr for the case study described in this paper); and c is
274 a parameter to adjust dependence according to duration. This adjustment is intended to condition the
275 behaviour of shorter duration extremes on a D -hour extreme of specified magnitude. It is constructed
276 to reflect the fact that when compared to a D -hour extreme, a shorter duration results in less extremal
277 dependence. Cases involving conditioning of longer periods on shorter periods (such as a 36 hr extreme
278 given a 9 hr extreme has occurred) can also use the relationship in Eq. (4), but with different parameter
279 values.

280 To fit the inverted max-stable process for all pairs of durations at locations x_1 and x_2 (i.e. 36 hr and 12
281 hr, 36 hr and 9 hr, 36 hr and 6 hr, 36 hr and 2 hr, 36 hr and 1 hr), the theoretical pairwise residual tail
282 dependence coefficient function in Eq. (3) is used with the adjusted variogram from Eq. (4) where the
283 parameters β and q are first obtained from the fitted results of the case of identical 36 hr durations at
284 location x_1 and x_2 . The parameter c is obtained by a least square fit of the residual tail dependence
285 coefficient across all durations.

286 ***4.3. Simulation based estimation of areal and joint rainfall***

287 The dependence model specification in the previous section enables the calculation of joint and
288 conditional probabilities (Appendix B). Therefore, in addition to traditional IDF return level maps that
289 are based on independence between locations and durations, it is possible to account for the coincidence
290 of rainfall within the region. Current design procedures using IDF estimates are event-based and rely
291 on ancillary steps to reconstruct elements of the design storm that were broken during the estimation
292 procedure. One critical element is the areal reduction factor (ARF), which can also be estimated by
293 using the dependence model. ARFs are used to adjust rainfall at a point (such as the centroid of a

294 catchment) to an effective mean rainfall over the catchment with equivalent probability of exceedance
295 ([Ball et al., 2016](#); [Le et al., 2018a](#)). ARFs can be estimated from observed rainfall data, but it is difficult
296 to extrapolate them for long return periods from observations with just 35 years of record for this study.
297 To deal with this difficulty and to analyse the asymptotic behaviour of ARFs, [Le et al. \(2018a\)](#) proposed
298 a framework to simulate ARFs using the same inverted-max stable process model adopted here. The
299 simulation procedure from [Le et al. \(2018a\)](#) is summarised according to two steps. In the first step, the
300 theoretical residual tail dependence coefficient function in Eq. (3) is fitted to observed rainfall for the
301 duration of interest to obtain the variogram parameters $q > 0$ and $\beta \in (0,2)$. The inverted Brown-
302 Resnick process is obtained from a simulation of the Brown-Resnick process using the algorithm of
303 [Dombry et al. \(2016\)](#) over a spatial domain. In the second step, the simulation in step 1 is transformed
304 from unit Fréchet margins to the rainfall scaled margins (inverse transformation of Eq. (B.1) in
305 Appendix B). For rainfall magnitudes above the threshold the generalised Pareto distribution in Eq. (1)
306 is used, and below the threshold the empirical distribution is used. The empirical distributions at
307 ungauged sites are derived from the nearest gauged sites and using the interpolated response surface of
308 the GPD threshold parameter.

309 An advantage of the simulation approach is that it can reflect the proportion of dry days in the empirical
310 distribution by making the simulated rainfall contain zero values ([Thibaud et al., 2013](#)). Another
311 advantage is that the use of empirical distributions guarantees that the marginal distributions of
312 simulated rainfall below the threshold match the observed marginal distributions. There may be a
313 drawback by forcing the simulated rainfall to have the same extremal dependence structure for both
314 parts below and above the threshold, which may not be true for non-extreme rainfall. However, the
315 dependence structure of non-extreme rainfall contributes insignificantly to extreme events ([Thibaud et](#)
316 [al., 2013](#)) and is unlikely to affect the results.

317 For calculating ARFs, the simulation is implemented separately for spatial rainfall of 36 and 9 hrs
318 duration. ARFs are calculated for each duration and different return periods, which can be found in the
319 supplementary material (Fig. S1 and S2). Figure S1 and S2 provide relationships between ARFs and
320 area (in km²) for different return periods for the case study catchments simulated using the inverted

321 Brown-Resnick process over equally sized grid points. The relationships are interpolated to obtain the
322 ARFs for each subcatchment.

323 The recommended approach for estimating the overall failure probability of a system is demonstrated
324 by considering a hypothetical traffic system with multiple river crossings at locations. If there is a one-
325 to-one correspondence between extreme rainfall intensity over a catchment and flood magnitude, the
326 overall failure probability will be approximately equal to the probability that there is at least one river
327 crossing whose contributing catchment has rainfall extremes exceeding the design level, which can be
328 estimated using simulations of the spatial rainfall model. Given the different times of concentration in
329 each catchment, the simulation must account for extremes of different durations. Specifically, the
330 covariance matrix of the simulation procedure provided by [Dombry et al. \(2016\)](#) is calculated from the
331 variogram in Eq. (3). The covariance element for a pair of locations with the same duration (e.g. 36 and
332 36 hr) is calculated from the variogram of identical durations for 36 and 36 hr. The covariance element
333 for a pair of locations with different durations, for example 36 and 9 hr, is calculated from the variogram
334 across durations for 36 and 9 hr. A set of 10,000 years simulated rainfall is generated from the fitted
335 model to calculate the overall failure probability of a highway section (Eq. B.5). The process is repeated
336 100 times to estimate the average failure probability, under the assumption that all river crossings of
337 the highway are designed to the same individual failure probability.

338 ***4.4. Transforming rainfall extremes to flood flow***

339 To estimate flood flow from rainfall extremes, the Watershed Bounded Network Model (WBNM)
340 ([Boyd et al., 1996](#)), is employed. WBNM calculates flood runoff from rainfall hyetographs that
341 represent the relationship between the rainfall intensity and time ([Chow et al., 1988](#)). It divides the
342 catchment into subcatchments, allowing hydrographs to be calculated at various points within the
343 catchment, and allowing the spatial variability of rainfall and rainfall losses to be modelled. It separates
344 overland flow routing from channel routing, allowing changes to either or both of these processes, for
345 example in urbanised catchments. The rainfall extremes are estimated at the centroid of the catchment,
346 and are converted to average spatial rainfall using the simulated ARFs described in Section 4.3. Design

347 rainfall hyetographs are used to convert the rainfall magnitude to absolute values through the duration
348 of a storm following standard design guidance in Australia ([Ball et al., 2016](#)).

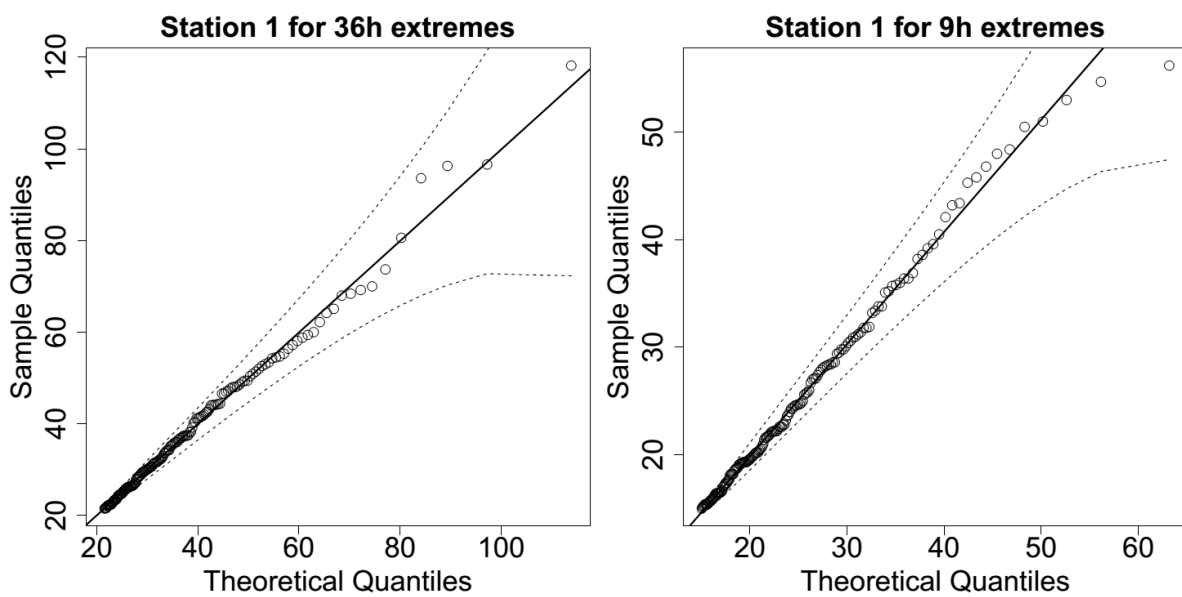
349 Hydrological models (WBNM) for the case study area were developed and calibrated in previous
350 studies ([WMAWater, 2011](#)). Hydrological model layouts for the Bellinger, Kalang River, Nambucca,
351 Warrell and Deep Creek catchments can be found in the supplementary material (Fig. S3 to S5).

352 5. Results

353 5.1. Evaluation of model for space-duration rainfall process

354 A GPD with an appropriate threshold was fitted to the observed rainfall data for 36 hr and 9 hr durations,
355 and the Brown-Resnick inverted max-stable process model was calibrated to determine the spatial
356 dependence.

357 Analysis of the rainfall records led to the selection of a threshold of 0.98 for all records as reasonable
358 across the spatial domain and the GPD was fitted to data above the selected threshold. Figure 5 shows
359 QQ plots of the marginal estimates for a representative station for two durations (36 and 9 hr). Overall
360 the quality of fitted distributions is good and plots for all other stations can be found in the
361 supplementary material (Fig. S6 and S7).

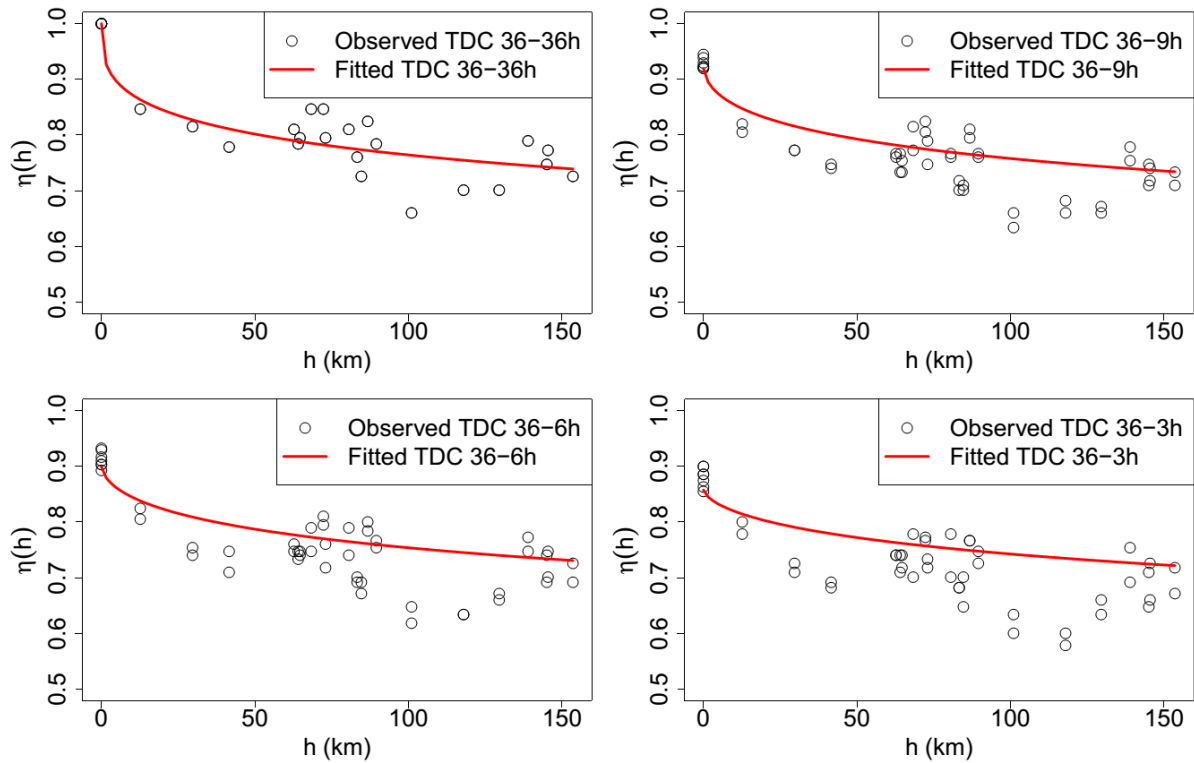


362

363 **Figure 5.** QQ plots for the fitted GPD at one representative station, dotted lines are the 95% confidence bounds, and the
364 solid diagonal line indicates a perfect fit.

365 The inverted max-stable process across different durations was calibrated to determine dependence
366 parameters. The theoretical pairwise residual tail dependence coefficient function between two
367 locations (x_1 and x_2) was calculated based on Eq. (3) and Eq. (4), and the observed pairwise residual
368 tail dependence coefficient η was calculated using Eq. (2). Figure 6 shows the pairwise residual tail
369 dependence coefficients for the Brown-Resnick inverted max-stable process versus distance. The black
370 points are the observed pairwise residual tail dependence coefficients, while the red lines are the fitted
371 pairwise residual tail dependence coefficient functions. A coefficient equal to 1 indicates complete
372 spatial dependence, and a value of 0.5 indicates complete spatial independence. The top-left panel
373 shows the dependence between 36 hr extremes across space, with the distance $h = 0$ corresponding to
374 “complete dependence”. It also shows the dependence decreasing with increasing distance. Figure 6
375 indicates that the model has a reasonable fit to the observed data given the small number of dependence
376 parameters. Although the theoretical coefficient (red line) does not perfectly match at long distances,
377 the main interest for this case study is in short distances, including at $h = 0$ for the case of dependence
378 between two different durations at the same location.

379 The remaining panels of Fig. 6 show the dependence of 36 vs. 9 hr extremes, 36 vs. 6 hr extremes, and
380 36 vs. 3 hr extremes, with the latter two duration combinations not being used directly in the study but
381 nonetheless showing the model performance across several durations. As expected, the dependence
382 levels are weaker compared with 36 vs. 36 hr extremes at the same distance, especially at zero distance.
383 This is expected, as extremes of different durations are more likely to arise from different storm events
384 compared to storms of the same duration.



385

386

387

388

389

390

391

392

393

394

395

396

397

398

399

400

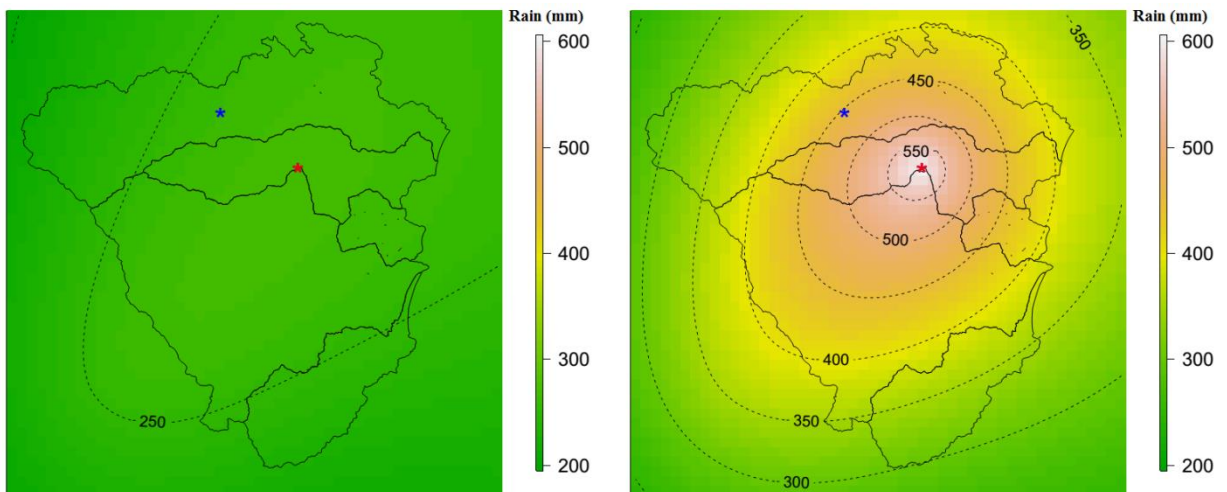
401

Figure 6. Plots of pairwise residual tail dependence coefficient (TDC) against distance for 36 hr extremes and 36 hr extremes (top left), for 36 hr extremes and 9 hr extremes (top right), for 36 hr extremes and 6 hr extremes (bottom left), and for 36 hr extremes and 3 hr extremes (bottom right). The black points are estimated residual tail dependence coefficients for pairs of sub-daily stations, and the red lines are theoretical residual tail dependence coefficient function.

5.2. Estimating conditional rainfall return levels and corresponding conditional flows for evacuation route design

The recommended approach for estimating conditional rainfall extremes is demonstrated by considering a hypothetical evacuation route across location x_2 , given a flood occurs at location x_1 , evaluated using Eq. (B.4). This approach is applied to a case study of the Pacific Highway upgrade project that contains five main river crossings (from Fig. 3). For evacuation purposes, we need to know “what is the probability that a bridge fails only once on average every M times (e.g., $M = 10$ for a one in 10 chance conditional event) when a neighbouring bridge is flooded?” This section provides the conditional estimates for two pairs of neighbouring bridges in the case study that have the shortest Euclidean distances, i.e. pairs (x_1, x_2) and (x_2, x_3) . The comparisons of unconditional and conditional maps are given in Fig. 7 and Fig. 8, and the corresponding unconditional and conditional flows are given in Fig. 9.

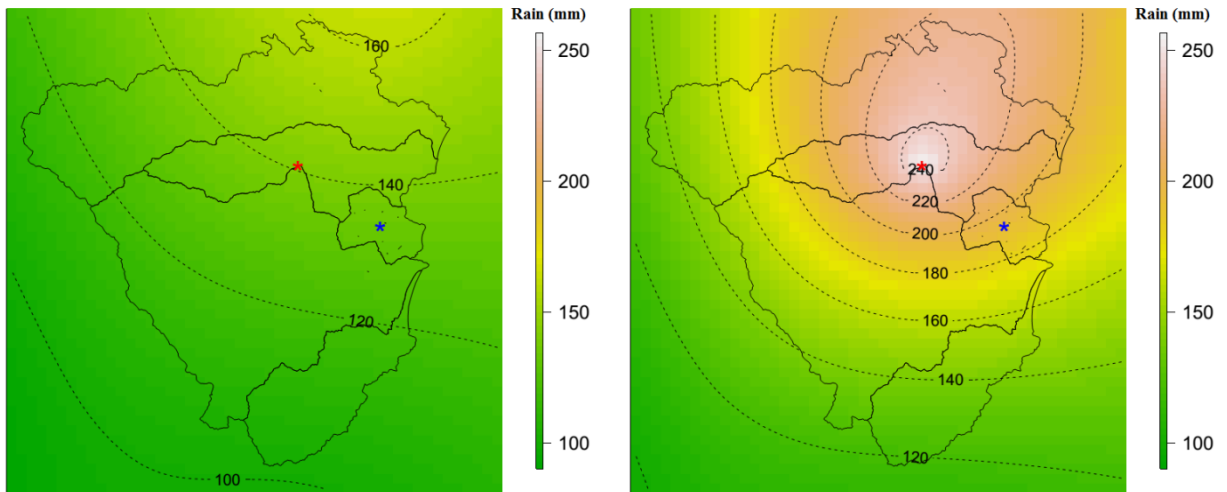
402 The left panel of Fig. 7 provides the pointwise 10-year unconditional return level map over the case
 403 study area for 36 hr rainfall extremes. The value at the location of interest—the blue star (the centroid
 404 of Bellinger catchment)—is around 260 mm. The right panel of Fig. 7 indicates that when accounting
 405 for the effect of a 20-year event for 36 hr rainfall extremes happening at the location of the red star (the
 406 centroid of Kalang River catchment), the pointwise one in 10 chance conditional return level at the blue
 407 star rises to around 453 mm (i.e., 1.74 times the unconditional value).



408
 409 **Figure 7.** Pointwise 10-year unconditional return level map (mm) for 36 hr extremes (left), and pointwise one in 10 chance
 410 conditional return level map (mm) for 36 hr extremes given a 20-year event for 36 hr extremes happen at location of the red
 411 star for the centroid of Kalang River catchment (right). The colour scales are the same for comparison.

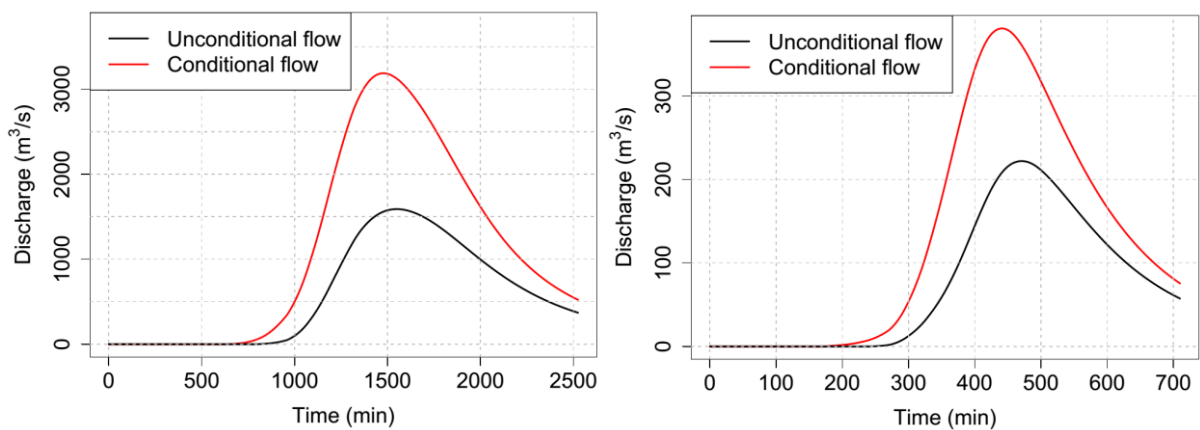
412 Figure 8 provides similar plots to Fig. 7 for another pair of locations having different durations of
 413 rainfall extremes due to different times of concentration in each catchment. Here, the location of interest
 414 is the centroid of the Deep Creek catchment (the blue star in Fig. 8) and the conditional point is the
 415 centroid of the Kalang River catchment (the red star in Fig. 8). The pointwise 10-year unconditional
 416 and one in 10 chance conditional return levels at the location of the blue star are 134 mm and 194 mm,
 417 respectively. The relative difference between the conditional and unconditional return levels is only
 418 1.45 times, compared with 1.74 times for the case in Fig. 7. This is because the pair of locations in Fig.
 419 8 has a longer distance than those in Fig. 7, so that the dependence level is weaker. Moreover, the
 420 location pair in Fig. 8 was analysed for different durations (between 36 and 9 hr extremes), which has

421 weaker dependence than the case of the equivalent durations in Fig. 7 (between 36 and 36 hr), based on
422 Fig. 6.



423
424 **Figure 8.** Pointwise 10-year unconditional return level map (mm) for 9 hr extremes (left), and pointwise one in 10 chance
425 conditional return level map (mm) for 9 hr extremes, given a 20-year event for 36 hr extremes happens at location of the red
426 star for the centroid of the Kalang River catchment (right). The colour scales are the same for comparison.

427 The unconditional and conditional return levels were extracted at the centroid of each main catchment,
428 and were converted to the absolute values of rainfall using a corresponding ARF and design storm
429 hyetograph. The unconditional and conditional flood flows at the river crossing in the Bellinger
430 catchment (corresponding to the unconditional and conditional rainfall extremes in Fig. 7) are given in
431 Fig. 9 (left panel). Similar plots for the river crossing in the Deep Creek catchment (corresponding to
432 the unconditional and conditional rainfall extremes in Fig. 8) are given in Fig. 9 (right panel).



433

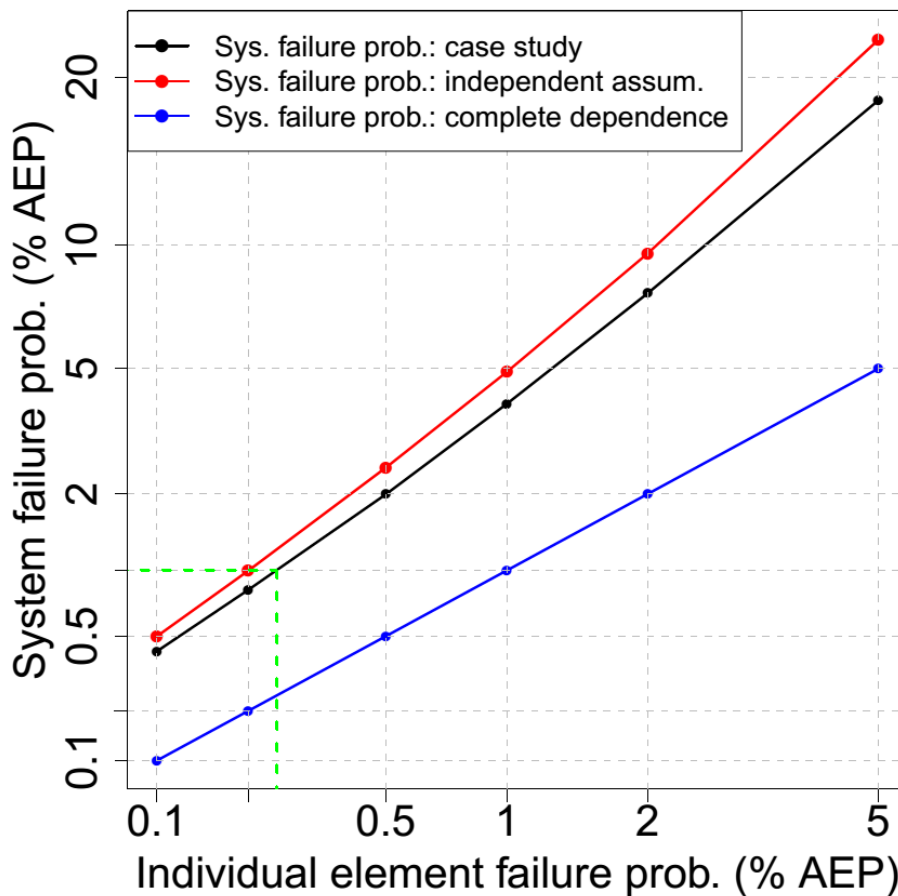
434 **Figure 9.** Comparison between conditional flows (red line) and unconditional flows (black line). (left) At the river crossing
435 in the Bellinger catchment (number 1 in Figure 3): conditional flow caused by an one in 10 chance conditional event for 36
436 hr rainfall in considering the effect of a 20-year event for 36 hr rainfall occurring at the river crossing in the Kalang River
437 catchment, and unconditional flow caused by a 10-year unconditional event for 36 hr. (right) At the river crossing in the
438 Deep Creek catchment (number 3 in Figure 3): conditional flow caused by an one in 10 chance conditional event for 9 hr
439 rainfall in considering the effect of a 20-year event for 36 hr rainfall occurring at the river crossing in the Kalang River
440 catchment, and unconditional flow caused by a 10-year unconditional event for 9 hr rainfall.

441 Fig. 9 presents peak flow for the Bellinger (left panel) and Deep Creek (right panel) catchments,
442 indicating that the peak conditional flow at the river crossings is almost 2.0 and 1.7 times higher than
443 the unconditional flow for the two catchments, respectively. This difference is a direct result of the
444 conditional event having a higher rainfall magnitude than the unconditional event: given that there is
445 an extreme event nearby, it is more likely for an extreme event to occur at a nearby location. If a bridge
446 design were to take into account this extra criterion for the purposes of evacuation planning it would
447 require the design to be at a higher level.

448 *5.3. Estimating the failure probability of the highway section based on the joint probability of rainfall* 449 *extremes*

450 Figure 10 is a plot of the overall failure probability of the highway as a function of the failure probability
451 of each individual river crossing (black). Similar relationships for the cases of complete dependence
452 (blue) and independence (red) are also provided for comparison. For the case of complete dependence,
453 when the whole region is extreme at the same time, the overall failure probability of the highway is
454 equal to the individual river crossing failure probability and it represents the lowest overall failure
455 probability. The worst case is complete independence where extremes do not happen together unless by
456 random chance; this means the failure probability of the highway is much higher than that for individual
457 river crossings. Taking into account the real dependence, there are some extremes that align and it seems
458 from Fig. 10 that this is a relatively weak effect. As an example from Fig. 10, to design the highway
459 with a failure probability of 1% annual exceedance probability (AEP), we would have to design each
460 individual river crossing to a much rarer AEP of 0.25% (see green lines in Fig. 10).

461



463

464 **Figure 10.** Relationship between system failure probability and individual element failure probability in % annual
 465 exceedance probability (% AEP). The black colour is for the case study, the red colour is for the case of independence, and
 466 the blue colour is for the case of complete dependence. The green lines help to interpolate the individual element failure
 467 probability from a given system failure probability of 1%. Both horizontal axis and vertical axis are constructed at a double
 468 log scale for viewing purposes.

469 6. Discussion and Conclusions

470 Hydrological design that is based on IDF estimates has conventionally focussed on separate estimation
 471 at single locations. Such an approach can lead to the misspecification of wider system risk of flooding
 472 since weather systems exhibit dependence in space, time and across storm durations, which can lead to
 473 the coincidence of extremes. A number of methods have been developed to address the problem of
 474 antecedent moisture within a single catchment, by accounting for the temporal dependence of rainfall
 475 at locations of interest through loss parameters or sampling rainfall patterns ([Rahman et al., 2002](#)).
 476 However, there have been fewer methods that account for the spatial dependence of rainfall across

477 multiple catchments, due in part to the complexity of representing the effects of spatial dependence in
478 risk calculations. Different catchments can have different times of concentration, so spatial dependence
479 may also imply the need to consider dependence across different durations of extreme rainfall bursts.

480 Recent and ongoing advances in modelling spatial rainfall extremes provide an opportunity to revisit
481 the scope of hydrological design. Such models include a max-stable model fitted using a Bayesian
482 hierarchical approach ([Stephenson et al., 2016](#)), max-stable and inverted max-stable models ([Nicolet et](#)
483 [al., 2017](#); [Padoan et al., 2010](#); [Russell et al., 2016](#); [Thibaud et al., 2013](#); [Westra and Sisson, 2011](#)) and
484 latent-variable Gaussian models ([Bennett et al., 2016b](#)). The ability to simulate rainfall over a region
485 means that hydrological problems need not be confined to individual catchments, but may cover
486 multiple catchments. Civil infrastructure systems such as highways, railways or levees are such
487 examples, since the failure of any one element may lead to overall failure of the system. Alternatively,
488 where there is a network, the failure of one element may have implications for the overall system to
489 accommodate the loss, by considering alternative routes. With models of spatial dependence and
490 duration dependence of extremes, there is a new and improved ability to address these problems
491 explicitly as part of the design methodology.

492 This paper demonstrated an application for evaluating conditional and joint probabilities of flood at
493 different locations. This was achieved with two examples: (i) the design of a river crossing that will fail
494 once on average every M times given that its neighbouring river crossing is flooded; and (ii) estimating
495 the probability that a highway section, which contains multiple river crossings, will fail based on the
496 failure probability of each individual river crossing. Due to the lack of continuous streamflow data and
497 sub-daily limitations of rain-based continuous simulation, this study used an event-based method of
498 conditional and joint rainfall extremes to estimate the corresponding conditional and joint flood flows.

499 The spatial rainfall was simulated using an asymptotically independent model, which was then used to
500 estimate conditional and joint rainfall extremes. Although this study focused on the inverted max-stable
501 model to simulate the extreme rainfall process, other methods such as the Gaussian copula may also be
502 appropriate and should be considered in future applications.

503 An empirical method was obtained from the framework of [Le et al. \(2018b\)](#) to make an asymptotically
504 independent model—the inverted max-stable process—able to capture the spatial dependence of rainfall
505 extremes across different durations. The fitted residual tail dependence coefficient function showed that
506 the model can capture the dependence for different pairs of durations. For our example, the highest ratio
507 of the one in 10 chance conditional event (in considering the effect of a 20-year event rainfall occurring
508 at the conditional location) to the 10-year unconditional event was 1.74, for the two catchments having
509 the strongest dependence (Fig. 7). The corresponding conditional flows were then estimated using a
510 hydrological model WBNM and shown to be strongly related to the ratio of conditional and
511 unconditional rainfall extremes (Fig. 9).

512 The joint probability of rainfall extremes for all catchments and for all possible pairs of catchments in
513 the case study area was estimated empirically from a set of 10,000 years of simulated rainfall extremes,
514 repeated 100 times to estimate the average value. The results showed that there were differences in the
515 failure probability of the highway after taking into account the rainfall dependence, but the effect was
516 not as emphatic as with the case of conditional probabilities. The difference in the failure probability
517 became weaker as the return period increased, which is consistent with the characteristic of
518 asymptotically independent data ([Ledford and Tawn, 1996](#); [Wadsworth and Tawn, 2012](#)). A
519 relationship was demonstrated (Fig. 10) to show how the design of the overall system to a given failure
520 probability requires the design of each individual river crossing to a rarer extremal level than when each
521 crossing is considered in isolation. For the case study example, it would be necessary to design each of
522 the five bridges to a 0.25% AEP event in order to obtain a system failure probability of 1%.

523 There is a need to reimagine the role of intensity-duration-frequency relationships. Conventionally they
524 have been developed as maps of the marginal rainfall in a point-wise manner for all locations and for a
525 range of frequencies and durations. The increasing sophistication of mathematical models for extremes,
526 computational power and interactive graphics abilities of online mapping platforms means that analysis
527 of hydrological extremes could significantly expand in scope. With an underlying model of spatial and
528 duration dependence between the extremes, it is not difficult to conceive of digital maps that
529 dynamically transform from the marginal representation of extremes to the corresponding

530 representation conditional extremes after any number of conditions are applied. This transformation is
531 exemplified by the differences between left and right panels in Fig. 7 and Fig. 8. Enhanced IDF maps
532 would enable a very different paradigm of design flood risk estimation, breaking away from analysing
533 individual system elements in isolation and instead emphasizing the behaviour of entire system.

534 **Appendix A. Calculation of empirical tail dependence coefficient**

535 To illustrate how Eq. (2) in the manuscript is calculated, consider a set of $n = 10$ observed values at
 536 the two locations: Z_1 and Z_2 (see Table A1). First, Z_1 and Z_2 are converted to empirical cumulative
 537 probability estimates via the Weibull plotting position formula $P = j/(n + 1)$ where j is ranked index
 538 of a data point giving P_1 and P_2 (see Table A1).

539 **Table A1.** Observed data Z_1 and Z_2 and corresponding empirical cumulative probabilities P_1 and P_2 .

Z_1	Z_2	P_1	P_2
5	10	0.455	0.909
9	1	0.818	0.091
1	7	0.091	0.636
2	6	0.182	0.545
10	4	0.909	0.364
3	3	0.273	0.273
8	9	0.727	0.818
6	2	0.545	0.182
4	8	0.364	0.727
7	5	0.636	0.455

540 Assume that interest is in values above a threshold u satisfying $P_u = 0.5$, in other words, $P\{Z_2 > u\} =$
 541 $P\{P_2 > P_u\} = 0.5$. In this case we have only one pair, at the index of 7, that satisfy both P_1 and P_2 are
 542 greater than $P_u = 0.5$, thus $P\{Z_1 > u, Z_2 > u\} = P\{P_1 > P_u, P_2 > P_u\} = 1/10 = 0.1$. The calculation
 543 of the empirical tail dependence coefficient is then

544
$$\eta(x_1, x_2) = \frac{\log P\{Z_2 > u\}}{\log P\{Z_1 > u, Z_2 > u\}} = \frac{\log P\{P_2 > P_u\}}{\log P\{P_1 > P_u, P_2 > P_u\}} = \frac{\log(0.5)}{\log(0.1)} = 0.301. \quad (A.1)$$

545

546 **Appendix B Estimate of conditional and joint probabilities of rainfall extremes**

547 The unit Fréchet transformation is given as

$$548 \quad z = \begin{cases} \left(\log \left\{ 1 - \Phi_u \left(1 + \frac{\xi(y-u)}{\sigma_u} \right)^{-1/\xi} \right\} \right)^{-1} & y > u, \xi \neq 0 \\ - \left(\log \left\{ 1 - \Phi_u \exp \left(-\frac{y-u}{\sigma_u} \right)^{-1/\xi} \right\} \right)^{-1} & y > u, \xi = 0 \\ -\{\log F(y_i)\}^{-1} & y \leq u \end{cases} \quad (B.1)$$

549 where y is the original marginal value and z is the Fréchet transformed value and all other parameters
 550 correspond to the GPD specified in Section 4.1. For values below the threshold, F is the empirical
 551 distribution function of y , $F(y_i) = i/(n+1)$ where i is the rank of y_i and n is the total number of data
 552 points.

553 The conditional probability $P\{Z_2 > z_2 | Z_1 > z_1\}$ is obtained from the bivariate inverted max-stable
 554 process cumulative distribution function (CDF) in unit Fréchet margins ([Thibaud et al., 2013](#)), which
 555 is given as:

$$556 \quad P\{Z_1 \leq z_1, Z_2 \leq z_2\} = 1 - \exp\left\{-\frac{1}{g_1}\right\} - \exp\left\{-\frac{1}{g_2}\right\} + \exp[-V\{g_1, g_2\}], \quad (B.2)$$

557 where $g_1 = -1/\log\{1 - \exp(-1/z_1)\}$, $g_2 = -1/\log\{1 - \exp(-1/z_2)\}$, and the exponent measure
 558 V ([Padoan et al., 2010](#)) is defined as:

$$559 \quad V\{g_1, g_2\} = -\frac{1}{g_1} \Phi\left\{\frac{a}{2} + \frac{1}{a} \log \frac{g_2}{g_1}\right\} - \frac{1}{g_2} \Phi\left\{\frac{a}{2} + \frac{1}{a} \log \frac{g_1}{g_2}\right\}. \quad (B.3)$$

560 In Eq. (B.3), Φ is the standard normal cumulative distribution function, $a = \sqrt{2\gamma_{ad}(h)}$ with $\gamma_{ad}(h)$ is
 561 the variograms that was mentioned in the explanation of Eq. (3).

562 In unit Fréchet margins, the relationship between the return level z and the return period T (in number
 563 of observations) is given as $z = -1/\log(1 - 1/T)$, and the conditional probability for the max-stable
 564 process can then be estimated using:

$$565 \quad P\{Z_2 > z_2 | Z_1 > z_1\} = T_1 \left[\frac{1}{T_1} - \exp\left(-\frac{1}{z_2}\right) + P\{Z_1 \leq z_1, Z_2 \leq z_2\} \right], \quad (B.4)$$

566 where T_1 is the return period (in number of observations for 36 hr rainfall) corresponding to the return
 567 level z_1 . It is also noted that in this paper Z_1 and Z_2 were taken as threshold exceedances, so the return
 568 period T_1 should be in the number of observations, which is equivalent to a $T_1/243$ -year return period
 569 because there are 243 observations for 36 hr rainfall in a year.

570 The probability that there is at least one location that has an extreme event exceeding a given threshold
 571 can be calculated based on the addition rule for the union of probabilities, as:

$$\begin{aligned}
 572 \quad P(Z_1 > z_1 \text{ or } \dots \text{ or } Z_N > z_N) &= \sum_{i=1}^N P(Z_i > z_i) - \sum_{i < j} P(Z_i > z_i, Z_j > z_j) + \dots \\
 573 \quad &+ (-1)^{N-1} P(Z_1 > z_1, \dots, Z_N > z_N), \tag{B.5}
 \end{aligned}$$

574 where N is the number of locations.

575 For the case of dependent variables, the joint probability for only two locations $P\{Z_1 > z_1, Z_2 > z_2\}$
 576 can be easily obtained from the bivariate CDF for inverted max-stable process in Eq. (B.2). However,
 577 for the case of multiple locations (five different locations for this paper), it is difficult to derive the
 578 formula for this probability because there are dependences between extreme events at all locations. So
 579 this probability is empirically calculated from a large number of simulations of the dependent model
 580 (see the description of the simulation procedure for an inverted max-stable process in Section 4.3).

581 For the case that all the events are independent, the joint probability for independent variables is broken
 582 down as the product of the marginals, and the conditional probability is equivalent to the marginal
 583 probability. When applying Eq. (B.5) for independent variables, the joint probability is therefore
 584 calculated by $P(Z_1 > z_1, \dots, Z_N > z_N) = P(Z_1 > z_1) \dots P(Z_N > z_N)$.

585 **Acknowledgments**

586 The lead author was supported by the Australia Awards Scholarships (AAS) from Australia
 587 Government. A/Prof Westra was supported by Australian Research Council Discovery grant
 588 DP150100411. We thank Mark Babister and Isabelle Testoni of WMA Water for providing the
 589 hydrologic models for the case study; and Leticia Mooney for her editorial help in improving this

590 manuscript. The rainfall data used in this study were provided by the Australian Bureau of Meteorology,
591 and can be obtained from the corresponding author.

592 **References**

- 593 Ball, J., Babister, M., Nathan, R., Weeks, W., Weinmann, E., Retallick, M., and Testoni, I.: Australian
594 Rainfall and Runoff: A Guide to Flood Estimation, © Commonwealth of Australia (Geoscience
595 Australia), 2016.
- 596 Bárdossy, A., and Pegram, G. G. S.: Copula based multisite model for daily precipitation simulation,
597 Hydrol. Earth Syst. Sci., 13, 2299-2314, 10.5194/hess-13-2299-2009, 2009.
- 598 Baxevani, A., and Lennartsson, J.: A spatiotemporal precipitation generator based on a censored latent
599 Gaussian field, Water Resources Research, 51, 4338-4358, doi:10.1002/2014WR016455, 2015.
- 600 Bennett, B., Lambert, M., Thyer, M., Bates, B. C., and Leonard, M.: Estimating Extreme Spatial
601 Rainfall Intensities, Journal of Hydrologic Engineering, 21, 04015074, doi:10.1061/(ASCE)HE.1943-
602 5584.0001316, 2016a.
- 603 Bennett, B., Thyer, M., Leonard, M., Lambert, M., and Bates, B.: A comprehensive and systematic
604 evaluation framework for a parsimonious daily rainfall field model, Journal of Hydrology,
605 <https://doi.org/10.1016/j.jhydrol.2016.12.043>, 2016b.
- 606 Bernard, M. M.: Formulas for rainfall intensities of long duration, Transactions of the American Society
607 of Civil Engineers, 96, 592-606, 1932.
- 608 Blanchet, J., and Creutin, J.-D.: Co-Occurrence of Extreme Daily Rainfall in the French Mediterranean
609 Region, Water Resources Research, 53, 9330-9349, 10.1002/2017wr020717, 2017.
- 610 Boughton, W., and Droop, O.: Continuous simulation for design flood estimation—a review,
611 Environmental Modelling & Software, 18, 309-318, [https://doi.org/10.1016/S1364-8152\(03\)00004-5](https://doi.org/10.1016/S1364-8152(03)00004-5),
612 2003.
- 613 Boyd, M. J., Rigby, E. H., and VanDrie, R.: WBNM — a computer software package for flood
614 hydrograph studies, Environmental Software, 11, 167-172, [https://doi.org/10.1016/S0266-
615 9838\(96\)00042-1](https://doi.org/10.1016/S0266-9838(96)00042-1), 1996.
- 616 Cameron, D. S., Beven, K. J., Tawn, J., Blazkova, S., and Naden, P.: Flood frequency estimation by
617 continuous simulation for a gauged upland catchment (with uncertainty), Journal of Hydrology, 219,
618 169-187, [https://doi.org/10.1016/S0022-1694\(99\)00057-8](https://doi.org/10.1016/S0022-1694(99)00057-8), 1999.
- 619 Carreau, J., Neppel, L., Arnaud, P., and Cantet, P.: Extreme Rainfall Analysis at Ungauged Sites in the
620 South of France : Comparison of Three Approaches, Journal de la Société Française de Statistique, 154
621 No. 2, 119-138, 2013.
- 622 Chow, V. T., Maidment, D. R., and Mays, L. W.: Applied Hydrology, McGraw-Hill, c1988, New York,
623 1988.
- 624 Coles, S., Heffernan, J., and Tawn, J.: Dependence Measures for Extreme Value Analyses, Extremes,
625 2, 339-365, 10.1023/a:1009963131610, 1999.
- 626 Coles, S.: An Introduction to Statistical Modeling of Extreme Values, Springer Series in Statistics,
627 Springer, 2001.
- 628 Davison, A. C., and Smith, R. L.: Models for exceedances over high thresholds, Journal of the Royal
629 Statistical Society. Series B (Methodological), 393-442, 1990.
- 630 de Haan, L.: A Spectral Representation for Max-stable Processes, The Annals of Probability, 12, 1194-
631 1204, 10.2307/2243357, 1984.
- 632 Demarta, S., and McNeil, A. J.: The t Copula and Related Copulas, International Statistical Review /
633 Revue Internationale de Statistique, 73, 111-129, 2005.
- 634 Dombry, C., Engelke, S., and Oesting, M.: Exact simulation of max-stable processes, Biometrika, 103,
635 303-317, 2016.
- 636 Durocher, M., Chebana, F., and Ouarda, T. B. M. J.: On the prediction of extreme flood quantiles at
637 ungauged locations with spatial copula, Journal of Hydrology, 533, 523-532,
638 <https://doi.org/10.1016/j.jhydrol.2015.12.029>, 2016.
- 639 Favre, A. C., Adlouni, S. E., Perreault, L., Thiémondge, N., and Bobée, B.: Multivariate hydrological
640 frequency analysis using copulas, Water Resources Research, 40, doi:10.1029/2003WR002456, 2004.

641 Gupta, A. S., and Tarboton, D. G.: A tool for downscaling weather data from large-grid reanalysis
642 products to finer spatial scales for distributed hydrological applications, *Environmental Modelling &*
643 *Software*, 84, 50-69, <https://doi.org/10.1016/j.envsoft.2016.06.014>, 2016.

644 He, Y., Bárdossy, A., and Zehe, E.: A review of regionalisation for continuous streamflow simulation,
645 *Hydrology and Earth System Sciences*, 15, 3539, 2011.

646 Hegnauer, M., Beersma, J., Van den Boogaard, H., Buishand, T., and Passchier, R.: Generator of
647 Rainfall and Discharge Extremes (GRADE) for the Rhine and Meuse basins; Final report of GRADE
648 2.0, Document extern project, 2014.

649 Hosking, J. R. M., and Wallis, J. R.: *Regional Frequency Analysis - An Approach Based on L-Moments*,
650 Cambridge University Press, Cambridge, UK, 1997.

651 Hüsler, J., and Reiss, R.-D.: Maxima of normal random vectors: Between independence and complete
652 dependence, *Statistics & Probability Letters*, 7, 283-286, [https://doi.org/10.1016/0167-7152\(89\)90106-](https://doi.org/10.1016/0167-7152(89)90106-5)
653 [5](https://doi.org/10.1016/0167-7152(89)90106-5), 1989.

654 Kao, S.-C., and Govindaraju, R. S.: Trivariate statistical analysis of extreme rainfall events via the
655 Plackett family of copulas, *Water Resources Research*, 44, doi:10.1029/2007WR006261, 2008.

656 Kleiber, W., Katz, R. W., and Rajagopalan, B.: Daily spatiotemporal precipitation simulation using
657 latent and transformed Gaussian processes, *Water Resources Research*, 48,
658 doi:10.1029/2011WR011105, 2012.

659 Koutsoyiannis, D., Kozonis, D., and Manetas, A.: A mathematical framework for studying rainfall
660 intensity-duration-frequency relationships, *Journal of Hydrology*, 206, 118-135,
661 [http://dx.doi.org/10.1016/S0022-1694\(98\)00097-3](http://dx.doi.org/10.1016/S0022-1694(98)00097-3), 1998.

662 Kuichling, E.: The relation between the rainfall and the discharge of sewers in populous districts,
663 *Transactions of the American Society of Civil Engineers*, 20, 1-56, 1889.

664 Laurenson, E. M., and Mein, R. G.: RORB Version 4 Runoff Routing Program User Manual, Monash
665 University Department of Civil Engineering, 1997.

666 Le, P. D., Davison, A. C., Engelke, S., Leonard, M., and Westra, S.: Dependence properties of spatial
667 rainfall extremes and areal reduction factors, *Journal of Hydrology*, 565, 711-719,
668 <https://doi.org/10.1016/j.jhydrol.2018.08.061>, 2018a.

669 Le, P. D., Leonard, M., and Westra, S.: Modeling Spatial Dependence of Rainfall Extremes Across
670 Multiple Durations, *Water Resources Research*, 54, 2233-2248, doi:10.1002/2017WR022231, 2018b.

671 Ledford, A. W., and Tawn, J. A.: Statistics for Near Independence in Multivariate Extreme Values,
672 *Biometrika*, 83, 169-187, 1996.

673 Leonard, M., Lambert, M. F., Metcalfe, A. V., and Cowpertwait, P. S. P.: A space-time Neyman–Scott
674 rainfall model with defined storm extent, *Water Resources Research*, 44, doi:10.1029/2007WR006110,
675 2008.

676 Leonard, M., Westra, S., Phatak, A., Lambert, M., Hurk, B. v. d., McInnes, K., Risbey, J., Schuster, S.,
677 Jakob, D., and Stafford-Smith, M.: A compound event framework for understanding extreme impacts,
678 *Wiley Interdisciplinary Reviews: Climate Change*, 5, 113-128, doi:10.1002/wcc.252, 2014.

679 Mulvaney, T. J.: On the use of self-registering rain and flood gauges in making observation of the
680 relation of rainfall and floods discharges in a given catchment, *Proc. Civ. Eng. Ireland*, 4, 18–31, 1851.

681 Nicolet, G., Eckert, N., Morin, S., and Blanchet, J.: A multi-criteria leave-two-out cross-validation
682 procedure for max-stable process selection, *Spatial Statistics*, 22, 107-128,
683 <https://doi.org/10.1016/j.spasta.2017.09.004>, 2017.

684 Padoan, S. A., Ribatet, M., and Sisson, S. A.: Likelihood-Based Inference for Max-Stable Processes,
685 *Journal of the American Statistical Association*, 105, 263-277, 10.1198/jasa.2009.tm08577, 2010.

686 Pathiraja, S., Westra, S., and Sharma, A.: Why continuous simulation? The role of antecedent moisture
687 in design flood estimation, *Water Resources Research*, 48, doi:10.1029/2011WR010997, 2012.

688 Pickands, J.: Statistical Inference Using Extreme Order Statistics, *The Annals of Statistics*, 3, 119-131,
689 10.2307/2958083, 1975.

690 Rahman, A., Weinmann, P. E., Hoang, T. M. T., and Laurenson, E. M.: Monte Carlo simulation of flood
691 frequency curves from rainfall, *Journal of Hydrology*, 256, 196-210, [https://doi.org/10.1016/S0022-](https://doi.org/10.1016/S0022-1694(01)00533-9)
692 [1694\(01\)00533-9](https://doi.org/10.1016/S0022-1694(01)00533-9), 2002.

693 Rasmussen, P. F.: Multisite precipitation generation using a latent autoregressive model, *Water*
694 *Resources Research*, 49, 1845-1857, doi:10.1002/wrcr.20164, 2013.

695 Renard, B., and Lang, M.: Use of a Gaussian copula for multivariate extreme value analysis: Some case
696 studies in hydrology, *Advances in Water Resources*, 30, 897-912,
697 <http://dx.doi.org/10.1016/j.advwatres.2006.08.001>, 2007.

698 Requena, A. I., Chebana, F., and Ouarda, T. B. M. J.: A functional framework for flow-duration-curve
699 and daily streamflow estimation at ungauged sites, *Advances in Water Resources*, 113, 328-340,
700 <https://doi.org/10.1016/j.advwatres.2018.01.019>, 2018.

701 Russell, B. T., Cooley, D. S., Porter, W. C., and Heald, C. L.: Modeling the spatial behavior of the
702 meteorological drivers' effects on extreme ozone, *Environmetrics*, 27, 334-344, doi:10.1002/env.2406,
703 2016.

704 Schlather, M.: Models for Stationary Max-Stable Random Fields, *Extremes*, 5, 33-44,
705 10.1023/A:1020977924878, 2002.

706 Seneviratne, S. I., Nicholls, N., Easterling, D., Goodess, C. M., Kanae, S., Kossin, J., Luo, Y., Marengo,
707 J., McInnes, K., and Rahimi, M.: Managing the Risks of Extreme Events and Disasters to Advance
708 Climate Change Adaptation: Changes in Climate Extremes and their Impacts on the Natural Physical
709 Environment, 2012.

710 Nambucca Heads Flood Study:
711 http://www.nambucca.nsw.gov.au/cp_content/resources/16152_2011_Nambucca_Heads_Flood_Study_Final_Draft_Chapter_6a.pdf, 2011.

712
713 Stedinger, J., Vogel, R., and Foufoula-Georgiou, E.: Frequency Analysis of Extreme Events, in:
714 Handbook of Hydrology, edited by: Maidment, D. R., McGraw-Hill, New York, 18.11-18.66, 1993.

715 Stephenson, A. G., Lehmann, E. A., and Phatak, A.: A max-stable process model for rainfall extremes
716 at different accumulation durations, *Weather and Climate Extremes*, 13, 44-53,
717 <https://doi.org/10.1016/j.wace.2016.07.002>, 2016.

718 Thibaud, E., Mutzner, R., and Davison, A. C.: Threshold modeling of extreme spatial rainfall, *Water
719 Resources Research*, 49, 4633-4644, 10.1002/wrcr.20329, 2013.

720 Wadsworth, J. L., and Tawn, J. A.: Dependence modelling for spatial extremes, *Biometrika*, 99, 253-
721 272, 10.1093/biomet/asr080, 2012.

722 Wang, Q. J.: A Bayesian Joint Probability Approach for flood record augmentation, *Water Resources
723 Research*, 37, 1707-1712, 10.1029/2000WR900401, 2001.

724 Wang, Q. J., Robertson, D. E., and Chiew, F. H. S.: A Bayesian joint probability modeling approach
725 for seasonal forecasting of streamflows at multiple sites, *Water Resources Research*, 45,
726 doi:10.1029/2008WR007355, 2009.

727 Wang, X., Gebremichael, M., and Yan, J.: Weighted likelihood copula modeling of extreme rainfall
728 events in Connecticut, *Journal of Hydrology*, 390, 108-115,
729 <http://dx.doi.org/10.1016/j.jhydrol.2010.06.039>, 2010.

730 Westra, S., and Sisson, S. A.: Detection of non-stationarity in precipitation extremes using a max-stable
731 process model, *Journal of Hydrology*, 406, 119-128, <http://dx.doi.org/10.1016/j.jhydrol.2011.06.014>,
732 2011.

733 WMAWater: Review of Bellinger, Kalang and Nambucca River Catchments Hydrology, Bellinger
734 Shire Council, Nambucca Shire Council, New South Wales Government, 2011.

735 Zhang, L., and Singh, V. P.: Gumbel–Hougaard Copula for Trivariate Rainfall Frequency
736 Analysis, *Journal of Hydrologic Engineering*, 12, 409-419, doi:10.1061/(ASCE)1084-
737 0699(2007)12:4(409), 2007.

738 Zheng, F., Westra, S., and Leonard, M.: Opposing local precipitation extremes, *Nature Clim. Change*,
739 5, 389-390, 10.1038/nclimate2579

740 <http://www.nature.com/nclimate/journal/v5/n5/abs/nclimate2579.html#supplementary-information>,
741 2015.

742 Zscheischler, J., Westra, S., van den Hurk, B. J. J. M., Seneviratne, S. I., Ward, P. J., Pitman, A.,
743 AghaKouchak, A., Bresch, D. N., Leonard, M., Wahl, T., and Zhang, X.: Future climate risk from
744 compound events, *Nature Climate Change*, 8, 469-477, 10.1038/s41558-018-0156-3, 2018.

745